Decomposition of the skin-friction coefficient of compressible boundary layers

Dongdong Xu (徐东东)[1], Pierre Ricco[1]* and Lian Duan[2]

[1]*Department of Mechanical Engineering,*
The University of Sheffield, Sheffield, S1 3JD, UK

[2]*Department of Mechanical and Aerospace Engineering,*
The Ohio State University, Columbus, Ohio 43210, USA

February 18, 2023

Abstract

Accepted for publication in Phys. Fluids (2023). DOI: 10.1063/5.0142129

We derive an integral formula for the skin-friction coefficient of compressible boundary layers by extending the formula of Elnahhas & Johnson (2022) for incompressible boundary layers. The skin-friction coefficient is decomposed into the sum of the contributions of the laminar coefficient, the change of the dynamic viscosity with the temperature, the Favre-Reynolds stresses and the mean flow. This decomposition is applied to numerical data for laminar and turbulent boundary layers and the role of each term on the wall-shear stress is quantified. We also show that the three-fold integration identity of Gomez *et al*. (2009) and the two-fold integration identities of Wenzel *et al*. (2022) and Xu *et al*. (2022) for turbulent boundary layers all simplify to the compressible von Kármán momentum integral equation when the upper limit of integration is asymptotically large. The dependence of these identities on the upper integration bound is studied. By using asymptotic methods, we prove that the multiple-integration identity of Wenzel *et al*. (2022) degenerates to the definition of the skin-friction coefficient when the number of integrations is asymptotically large.

1 Introduction

The skin friction of turbulent boundary layers is usually much larger than that of laminar boundary layers. The high turbulent skin friction causes a large dissipation of kinetic energy into heat and

*corresponding author: p.ricco@sheffield.ac.uk

thus a loss of performance in an immense range of aerodynamics applications in industry and technology. The underlying physical mechanisms responsible for the large skin friction in turbulent wall-bounded flows have therefore attracted the interest of engineers and scientists.

The skin friction of wall-bounded shear flows can be calculated directly by multiplying the dynamic viscosity and the wall-normal gradient of the streamwise velocity at the wall. However, the latter quantity is extremely difficult to measure and therefore researchers have devoted effort to finding alternative approaches that can give further useful information about the physical mechanisms. In one such effort, Fukagata et al. (2002) (FIK) obtained an integral identity that, for incompressible channel and pipe flows, expresses the scaled wall-shear stress as the sum of the laminar skin-friction coefficient and a weighted integral of the Reynolds stresses. An additional integral term is present in the case of free-stream boundary layers because of their streamwise inhomogeneity. In the latter flows, which are external and spatially-developing, the upper bound of integration is not defined precisely and, as shown for example by Ricco and Skote (2022), the contribution of the terms depends significantly on this upper bound. If the upper integration bound is taken to be asymptotically large, Ricco and Skote (2022) proved that the FIK identity reduces to the so-called von Kármán momentum integral equation (von Kármán, 1946), which links the skin-friction coefficient to the streamwise change of the momentum thickness. The Reynolds stresses thus disappear from the identity. Ricco and Skote (2022) concluded that the impact of the Reynolds stresses on the wall-shear stress of turbulent boundary layers cannot be quantified via the FIK identity because the dependence on the integration limit is spurious. They also discussed how other variants of the original FIK identity for free-stream boundary layers showed this dependence on the upper bound of integration.

An alternative identity was derived from the mean kinetic energy equation by Renard and Deck (2016) (RD) for free-stream boundary layers. The upper integration bound is infinite in this case and therefore the RD decomposition does not suffer from the issue related to the integration bound pertaining to the FIK identity. The skin-friction coefficient can thus be successfully decomposed and physically interpreted as the sum of the terms in the energy budget. Elnahhas and Johnson (2022) (EJ) decomposed the skin-friction coefficient of incompressible boundary layers in a sum of terms related to the laminar boundary layer, the Reynolds stresses and the mean-flow inhomogeneity. They identified a quantity, function of the streamwise direction, as a preferred position in the boundary layer around which the angular momentum exerted by the flow can be computed. It is not straightforward to arrive at an identity for free-stream boundary layers that uniquely quantifies the contribution of turbulence in a single term because the turbulent fluctuations, besides inducing the Reynolds stresses, also modify the mean flow. An analogous difficulty is encountered when the contribution of compressibility has to be quantified.

The study of wall friction exerted by compressible turbulent boundary layers is more complicated than in the incompressible regime because of the intrinsic coupling of momentum and energy transfer. Gomez et al. (2009) (GFS) extended the FIK identity to the cases of compressible wall-bounded flows. They decomposed the skin-friction coefficient as the sum of four

terms, two of which pertain to the flow compressibility. However, the effect of compressibility was not distilled in a single term because of the change in mean density. The RD identity was extended to the compressible cases by Fan et al. (2019). Wenzel et al. (2022) (WGK) and Xu et al. (2022) (XWC) obtained alternative identities for compressible boundary layers by utilizing a two-fold integration, instead of a three-fold integration as in the original FIK study. Compared with the three-fold integration method, the two-fold integration method eliminates the wall-distance-dependent term in the integral containing the Reynolds stresses.

Ricco and Skote (2022) performed multiple integrations on the incompressible streamwise momentum equation to extend the original FIK identities. They showed that the resulting FIK-like identities also simplify to the von Kármán momentum integral equation. The repeated integration was performed by WGK in the compressible regime, where the upper bound of integration exceeded the boundary-layer thickness because the influence of the thermal boundary layer had to be considered. The impact of the upper bound of integration for compressible FIK-like identities remains an open research point.

In this paper, we first extend the method of EJ to the study of the skin-friction coefficient of compressible boundary layers. The Favre-averaged equation is used to derive the integral equation. The decomposition identity is derived in §2 and the results of the decomposition in the laminar and the turbulent cases are discussed in §3.1 and §3.2, respectively. We also extend the work of Ricco and Skote (2022) to the compressible regime. In §4.1 and §4.2, we prove that the three-fold GFS identity and the two-fold identities by WGK and XWC all possess a spurious dependence on the upper integration bound and simplify to the compressible von Kármán integral equation when the upper bound is infinitely large. In §4.3, the successive-integration WGK identity is shown to collapse to the definition of the skin-friction coefficient when the number of integration is infinitely large, thus showing how the dependence of the terms on the number of integration is spurious. Concluding remarks are contained in §5.

2 Theoretical framework

We consider a compressible boundary layer over a flat plate where x^*, y^* and z^* are the streamwise, wall-normal and spanwise directions, respectively. The flat plate is at $y^* = 0$ and the leading edge of the plate is at $x^* = 0$. The velocity components along x^*, y^* and z^* are u^*, v^* and w^*, respectively. The Navier-Stokes equations are scaled by using the free-stream velocity at $x^* = 0$, $\mathcal{U}^*_\infty$, as the reference velocity and a length $\mathcal{L}^*$ as the reference length scale. The temperature T^*, the density ρ^* and the dynamic viscosity μ^* are scaled by their respective free-stream values at $x^* = 0$, i.e. T^*_∞, ρ^*_∞ and μ^*_∞ . The time t^* and the pressure p^* are scaled by $\mathcal{L}^*/\mathcal{U}^*_\infty$ and $\rho^*_\infty \mathcal{U}^{*2}_\infty$, respectively. The asterisk $*$ denotes dimensional quantities, while quantities without any symbol are non-dimensional. The subscripts ∞ and e indicate free-stream quantities at $x^* = 0$ and at the outer edge of the boundary layer, respectively. The Prandtl number Pr and the ratio of specific heats γ are taken as constants. The free-stream potential flow is isentropic and the free-stream

density and temperature are constant, i.e. $T_e = \rho_e = 1$.

Reynolds-averaging a quantity q over z along a distance $\mathcal{L}_z$ and over t for a time interval $\mathcal{T}$ is defined as

$$\bar{q}(x,y) = \frac{1}{\mathcal{T}\mathcal{L}_z}\int_0^{\mathcal{T}}\int_0^{\mathcal{L}_z} q(x,y,z,t)\mathrm{d}z\mathrm{d}t. \tag{2.1}$$

Favre-averaging is also adopted to attain a simplified form for the convective terms of the Navier-Stokes equations (Favre, 1965, 1992). A Favre-averaged quantity is defined as

$$\langle q\rangle = \frac{\overline{\rho q}}{\bar{\rho}}. \tag{2.2}$$

The flow is decomposed as

$$q(x,y,z,t) = \bar{q}(x,y) + q'(x,y,z,t) = \langle q\rangle(x,y) + q''(x,y,z,t). \tag{2.3}$$

A Favre-averaged quantity satisfies $\overline{\rho q''} = 0$ and $\overline{\rho\langle q\rangle q''} = 0$. Auxiliary relations include

$$\overline{\rho\langle q\rangle} = \bar{\rho}\langle q\rangle = \overline{\rho q}, \quad \langle q_i q_j\rangle = \langle q_i\rangle\langle q_j\rangle + \langle q_i'' q_j''\rangle. \tag{2.4}$$

The relation between the Reynolds average and the Favre average is

$$\langle q\rangle - \bar{q} = q' - q'' = \frac{\overline{\rho' q''}}{\bar{\rho}} = \frac{\overline{\rho' q'}}{\bar{\rho}}. \tag{2.5}$$

The Favre-averaged continuity and momentum equations for compressible, statistical two-dimensional flows are (Adumitroaie et al., 1999)

$$\left.\begin{aligned} \frac{\partial\bar{\rho}\langle u_j\rangle}{\partial x_j} &= 0, \\ \frac{\partial\bar{\rho}\langle u_i\rangle\langle u_j\rangle}{\partial x_j} + \frac{\partial\bar{\rho}\langle u_i'' u_j''\rangle}{\partial x_j} &= -\frac{\partial\bar{p}}{\partial x_i} + \frac{\partial\bar{\sigma}_{ji}}{\partial x_j}, \end{aligned}\right\} \tag{2.6}$$

where σ_{ji} is the stress tensor

$$\sigma_{ji} = \frac{2\mu}{Re}\left(S_{ij} - \frac{S_{kk}}{3}\delta_{ij}\right) \quad \text{with} \quad S_{ij} = \frac{1}{2}\left(\frac{\partial u_i}{\partial x_j} + \frac{\partial u_j}{\partial x_i}\right). \tag{2.7}$$

The Einstein summation convention is adopted to any Latin suffix occurring twice in a single-term expression. The Mach number and the Reynolds number are defined as

$$\mathcal{M}_\infty = \frac{\mathcal{U}_\infty^*}{\sqrt{\gamma R^* T_\infty^*}}, \quad Re = \frac{\rho_\infty^* \mathcal{U}_\infty^* \mathcal{L}^*}{\mu_\infty^*}, \tag{2.8}$$

where $R^* = 287.05$ J kg^{-1}K^{-1} is the ideal gas constant.

We now derive the relationship between the skin-friction coefficient and integral terms emerging from the x-momentum equation. The Favre-averaged x-momentum equation is rewritten as

$$\frac{\partial \bar{\rho}\langle u\rangle\langle u\rangle}{\partial x} + \frac{\partial}{\partial y}\left(\bar{\rho}\langle u\rangle\langle v\rangle + \bar{\rho}\langle u''v''\rangle - \frac{\bar{\mu}}{Re}\frac{\partial \bar{u}}{\partial y}\right) + I_x = 0. \tag{2.9}$$

where

$$I_x = \frac{\partial \bar{\rho}\langle u''u''\rangle}{\partial x} - \frac{\partial \bar{\sigma}_{xx}}{\partial x} - \left[\frac{\partial \bar{\sigma}_{yx}}{\partial y} - \frac{1}{Re}\frac{\partial}{\partial y}\left(\bar{\mu}\frac{\partial \bar{u}}{\partial y}\right)\right] + \frac{\partial \bar{p}}{\partial x}. \tag{2.10}$$

To help our derivation, the leading-order term $-Re^{-1}(\partial/\partial y)\,(\bar{\mu}\partial\bar{u}/\partial y)$, contained in $-\partial\bar{\sigma}_{yx}/\partial y$, is isolated in (2.9) and subtracted in (2.10).

In the free stream, the inviscid momentum equation is

$$\rho_e \mathcal{U}_e \frac{\mathrm{d}\mathcal{U}_e}{\mathrm{d}x} = -\frac{\mathrm{d}\mathcal{P}_e}{\mathrm{d}x}, \tag{2.11}$$

where $\mathcal{P}_e$ is the mean pressure. Subtracting (2.11) from (2.9) leads to the streamwise momentum deficit equation,

$$\begin{aligned}\frac{\partial(\langle u\rangle - \mathcal{U}_e)\bar{\rho}\langle u\rangle}{\partial x} + \frac{\partial}{\partial y}\left[(\langle u\rangle - \mathcal{U}_e)\bar{\rho}\langle v\rangle + \bar{\rho}\langle u''v''\rangle - \frac{\bar{\mu}}{Re}\frac{\partial \bar{u}}{\partial y}\right] \\ +(\bar{\rho}\langle u\rangle - \rho_e\mathcal{U}_e)\frac{\partial \mathcal{U}_e}{\partial x} + J_x = 0,\end{aligned} \tag{2.12}$$

where

$$J_x = \frac{\partial \bar{\rho}\langle u''u''\rangle}{\partial x} - \frac{\partial \bar{\sigma}_{xx}}{\partial x} - \left[\frac{\partial \bar{\sigma}_{yx}}{\partial y} - \frac{1}{Re}\frac{\partial}{\partial y}\left(\bar{\mu}\frac{\partial \bar{u}}{\partial y}\right)\right] + \frac{\partial(\bar{p} - \mathcal{P}_e)}{\partial x}. \tag{2.13}$$

In a high-Reynolds-number boundary layer, the first, second and last terms in (2.13) are negligible. The difference between the wall-normal viscous terms in (2.13) leads to the term $(\partial/\partial y)\left(\overline{\mu'\partial u'/\partial y}\right)$, which has been verified numerically to be very small in the boundary layer and zero at the wall for an isothermal wall. The compressible von Kármán momentum integral equation can be obtained by integrating (2.12) with respect to y from zero to infinity, as shown in Appendix A.

The local skin-friction coefficient is defined as in (6.59) of Anderson (2000),

$$\frac{C_f}{2} = \frac{\bar{\mu}^*}{\rho_e^*\mathcal{U}_e^{*2}}\left.\frac{\partial \bar{u}^*}{\partial y^*}\right|_{y^*=0} = \frac{\bar{\mu}}{\rho_e\mathcal{U}_e^2 Re}\left.\frac{\partial \bar{u}}{\partial y}\right|_{y^*=0}. \tag{2.14}$$

As in the study of EJ, the skin-friction integral equation is obtained by multiplying (2.12) by $y - \mathscr{C}$ and integrating the resulting equation along y from 0 to ∞, where $\mathscr{C}(x)$ is a length to be

determined. Dividing the results by $\rho_e \mathcal{U}_e^2 \mathscr{C}$ leads to

$$\begin{aligned}\frac{C_f}{2} &= \underbrace{\frac{1}{Re_{\mathscr{C}}}}_{C_l} + \underbrace{\frac{-1}{Re_{\mathscr{C}}\mathcal{U}_e\mu_e}\int_0^\infty \frac{\partial \bar{\mu}}{\partial y}\bar{u}\mathrm{d}y}_{C_{\bar{\mu}}} + \underbrace{\int_0^\infty \frac{-\bar{\rho}\langle u''v''\rangle}{\rho_e \mathcal{U}_e^2 \mathscr{C}}\mathrm{d}y}_{C_{tur}} + \underbrace{\frac{\mathrm{d}\theta_{\mathscr{C}}}{\mathrm{d}x} - \frac{\theta-\theta_{\mathscr{C}}}{\mathscr{C}}\frac{\mathrm{d}\mathscr{C}}{\mathrm{d}x}}_{C_\theta} \\ &+ \underbrace{\frac{\theta_v}{\mathscr{C}}}_{C_{\theta_v}} + \underbrace{\frac{\delta_{\mathscr{C}}+2\theta_{\mathscr{C}}}{\mathcal{U}_e}\frac{\mathrm{d}\mathcal{U}_e}{\mathrm{d}x}}_{C_p} + \underbrace{K_x}_{\text{High-order terms}}, \end{aligned} \tag{2.15}$$

where

$$Re_{\mathscr{C}}(x^*) = \frac{\rho_e^* \mathcal{U}_e^* \mathscr{C}^*(x^*)}{\mu_e^*} = \frac{\rho_e \mathcal{U}_e \mathscr{C}}{\mu_e} Re, \quad K_x \equiv \int_0^\infty \left(1-\frac{y}{\mathscr{C}}\right)\frac{J_x}{\rho_e \mathcal{U}_e^2}\mathrm{d}y, \tag{2.16}$$

$$\delta_{\mathscr{C}}(x) \equiv \int_0^\infty \left(1-\frac{y}{\mathscr{C}}\right)\left(1-\frac{\bar{\rho}\langle u\rangle}{\rho_e \mathcal{U}_e}\right)\mathrm{d}y, \;\; \theta_{\mathscr{C}}(x) \equiv \int_0^\infty \left(1-\frac{y}{\mathscr{C}}\right)\left(1-\frac{\langle u\rangle}{\mathcal{U}_e}\right)\frac{\bar{\rho}\langle u\rangle}{\rho_e \mathcal{U}_e}\mathrm{d}y \tag{2.17}$$

and

$$\begin{aligned}\frac{\mathrm{d}\theta_{\mathscr{C}}}{\mathrm{d}x} &= \int_0^\infty \frac{y}{\mathscr{C}^2}\frac{\mathrm{d}\mathscr{C}}{\mathrm{d}x}\left(1-\frac{\langle u\rangle}{\mathcal{U}_e}\right)\frac{\bar{\rho}\langle u\rangle}{\rho_e \mathcal{U}_e}\mathrm{d}y - \int_0^\infty \left(1-\frac{y}{\mathscr{C}}\right)\frac{\partial}{\partial x}\left(\frac{\langle u\rangle}{\mathcal{U}_e}\right)\frac{\bar{\rho}\langle u\rangle}{\rho_e \mathcal{U}_e}\mathrm{d}y \\ &+ \int_0^\infty \left(1-\frac{y}{\mathscr{C}}\right)\left(1-\frac{\langle u\rangle}{\mathcal{U}_e}\right)\frac{\partial}{\partial x}\left(\frac{\bar{\rho}\langle u\rangle}{\rho_e \mathcal{U}_e}\right)\mathrm{d}y. \end{aligned} \tag{2.18}$$

As in the incompressible case by EJ, the key step is to choose the length scale $\mathscr{C}(x)$ in such a way to render the first term on the right-hand-side of (2.15) equal to the skin-friction coefficient of the laminar boundary layer. This procedure is detailed in the discussion following (2.19). In (2.15), the term $C_{\bar{\mu}}$ indicates the contribution of the mean flow due to the variation of viscosity. The term C_{tur} is caused by the Favre-Reynolds stresses. The term C_θ is due to the spatial growth of the momentum thickness and the length $\mathscr{C}$. The terms C_{θ_v} and C_P result from the wall-normal velocity and the streamwise pressure gradient, respectively. The last term on the right-hand-side of (2.15), K_x, contains all the high-order terms, which are negligible in the limit of high Reynolds number.

We now discuss the derivation of each term of (2.15), following the integration of (2.12).

- Viscous stresses and laminar friction contribution

$$\begin{aligned}\frac{1}{Re}\int_0^\infty (y-\mathscr{C})\frac{\partial}{\partial y}\left(\bar{\mu}\frac{\partial \bar{u}}{\partial y}\right)\mathrm{d}y &= \frac{\mathscr{C}}{Re}\left(\bar{\mu}\frac{\partial \bar{u}}{\partial y}\right)\Big|_{y=0} - \frac{1}{Re}\int_0^\infty \bar{\mu}\frac{\partial \bar{u}}{\partial y}\mathrm{d}y \\ &= \rho_e \mathcal{U}_e^2 \mathscr{C}\frac{C_f}{2} - \frac{\mu_e \mathcal{U}_e}{Re} + \frac{1}{Re}\int_0^\infty \frac{\partial \bar{\mu}}{\partial y}\bar{u}\mathrm{d}y. \end{aligned} \tag{2.19}$$

The last term in (2.19) is induced by the variation of the dynamic viscosity due to the temperature gradient. It is null in the incompressible regime since the dynamic viscosity is constant.

For the special case of a laminar compressible boundary layer over a flat plate, the solution is self-similar and the skin-friction coefficient is given in (6.76) of Anderson (2000), namely,

$$\frac{C_f}{2} = \frac{\mathcal{F}(\mathcal{M}_e, T_w)}{\sqrt{Re_x}}, \tag{2.20}$$

where $Re_x = \rho^*_\infty \mathcal{U}^*_\infty x^*/\mu^*_\infty$. We adopt an appropriate $\mathscr{C}$ such that

$$\frac{C_f}{2} = \frac{1}{Re_{\mathscr{C}}} = \frac{\bar{\mu}}{\rho_e \mathcal{U}_e^2 Re} \frac{\partial \bar{u}}{\partial y}\bigg|_{y=0} = \frac{\mu_w \mathrm{d}^2 F/\mathrm{d}\eta^2|_{\eta=0}}{\rho_e \mathcal{U}_e^2 Re\ sT_w} \quad \text{with} \quad s = \sqrt{\frac{2x}{Re}}, \tag{2.21}$$

where $F(\eta)$ is the self-similar variable related to the laminar-flow velocity components, η is the scaled wall-normal coordinate and the subscript w denotes quantities at the wall, as detailed in Appendix B. In (2.21), the definition of η, given in Appendix B, has been used. For boundary layers with no pressure gradient, $\mathcal{U}_e = 1$. The laminar contribution can be isolated from the skin-friction coefficient (2.15) by choosing

$$\mathscr{C}(x) = \frac{sT_w}{\mu_w \mathrm{d}^2 F/\mathrm{d}\eta^2|_{\eta=0}}. \tag{2.22}$$

For an incompressible boundary layer, equation (2.22) reduces to

$$\mathscr{C} = \frac{s}{\mathrm{d}^2 F/\mathrm{d}\eta^2|_{\eta=0}} = 3.01\sqrt{\frac{x}{Re}}, \tag{2.23}$$

as given in EJ.

- Favre-Reynolds stresses

$$\int_0^\infty (y - \mathscr{C}) \frac{\partial \bar{\rho}\langle u''v''\rangle}{\partial y} \mathrm{d}y = -\int_0^\infty \bar{\rho}\langle u''v''\rangle \mathrm{d}y. \tag{2.24}$$

- Streamwise momentum flux

$$\int_0^\infty (y - \mathscr{C}) \frac{\partial (\langle u\rangle - \mathcal{U}_e)\bar{\rho}\langle u\rangle}{\partial x} \mathrm{d}y = \rho_e \mathcal{U}_e^2 \mathscr{C} \left(\frac{\mathrm{d}\theta_{\mathscr{C}}}{\mathrm{d}x} - \frac{\theta - \theta_{\mathscr{C}}}{\mathscr{C}} \frac{\mathrm{d}\mathscr{C}}{\mathrm{d}x} + \frac{2\theta_{\mathscr{C}}}{\mathcal{U}_e} \frac{\mathrm{d}\mathcal{U}_e}{\mathrm{d}x} \right), \tag{2.25}$$

where

$$\theta_{\mathscr{C}}(x) \equiv \int_0^\infty \left(1 - \frac{y}{\mathscr{C}}\right) \left(1 - \frac{\langle u\rangle}{\mathcal{U}_e}\right) \frac{\bar{\rho}\langle u\rangle}{\rho_e \mathcal{U}_e} \mathrm{d}y, \quad \theta(x) \equiv \int_0^\infty \left(1 - \frac{\langle u\rangle}{\mathcal{U}_e}\right) \frac{\bar{\rho}\langle u\rangle}{\rho_e \mathcal{U}_e} \mathrm{d}y. \tag{2.26}$$

- Wall-normal momentum flux

$$\int_0^\infty (y-\mathscr{C})\frac{\partial(\langle u\rangle-\mathcal{U}_e)\bar{\rho}\langle v\rangle}{\partial y}\mathrm{d}y=\rho_e\mathcal{U}_e^2\theta_v \;\text{ with }\; \theta_v\equiv\int_0^\infty\left(1-\frac{\langle u\rangle}{\mathcal{U}_e}\right)\frac{\bar{\rho}\langle v\rangle}{\rho_e\mathcal{U}_e}\mathrm{d}y. \tag{2.27}$$

- Pressure gradient contribution

$$\int_0^\infty (y-\mathscr{C})(\bar{\rho}\langle u\rangle-\rho_e\mathcal{U}_e)\frac{\mathrm{d}\mathcal{U}_e}{\mathrm{d}x}\mathrm{d}y=\rho_e\mathcal{U}_e\mathscr{C}\frac{\mathrm{d}\mathcal{U}_e}{\mathrm{d}x}\delta_{\mathscr{C}}. \tag{2.28}$$

The identity (2.15) is related to the compressible von Kármán momentum integral equation. In the limit $\mathscr{L}\to\infty$ (and hence $Re_{\mathscr{L}}\to\infty$), the first three terms on the right of (2.15) and the term C_{θ_v} are null. In this limit, the terms $\theta_{\mathscr{L}}$ and $\delta_{\mathscr{L}}$ simplify to the momentum thickness θ and the displacement thickness δ, defined in Appendix A, since $y/\mathscr{L}\ll 1$, and the term C_θ simplifies to $\mathrm{d}\theta/\mathrm{d}x$ because the second term of C_θ is null. By neglecting the high-order terms in the limit of large Reynolds number, the identity (2.15) thus simplifies to the compressible von Kármán momentum integral equation, given in (A.2), analogous to the incompressible case studied by EJ.

3 Numerical results

3.1 Skin-friction coefficient of laminar boundary layers

We first present the numerical results of the decomposition of the skin-friction coefficient for compressible self-similar laminar boundary layers without a streamwise pressure gradient. The free-stream Mach number is related to the Reynolds number as follows

$$Re=\frac{\mathcal{M}_\infty\rho_\infty^*\mathcal{L}^*}{\sqrt{\gamma R^*T_\infty^*}\mu_\infty^*(T_\infty^*)}. \tag{3.1}$$

In experiments, the Mach number can be fixed by changing the Reynolds number through an adjustment of the total pressure (Huang et al., 2021). The governing equations for a laminar boundary layer are discussed in Appendix B. The decomposed terms for the laminar flow are simplified to (B.4) in Appendix B. The dependence of the scaled wall-shear stress $\mathrm{d}^2F/\mathrm{d}\eta^2|_{\eta=0}$ on the Mach number is shown in figures 1(a) and 1(b) for an isothermal wall ($T_w=1$) and an adiabatic wall ($\partial T/\partial y|_{y=0}=0$), respectively. The Reynolds number is Re =1124, a typical value in turbomachinery experiments (Marensi et al., 2017). We choose a maximum Mach number equal to 6 in order to study the Mach-number effect.

Equation (2.21) indicates that the following parameter can be utilized to describe the skin-friction coefficient of laminar boundary layers, namely,

$$C_{f,R}=sReC_f=\sqrt{2xRe}C_f\,. \tag{3.2}$$

This parameter is a better choice for the investigation of the skin friction of laminar boundary layers since it excludes the effect of the Reynolds number and the streamwise coordinate from the skin-friction coefficient. Figure 1(c) and 1(d) display the decomposition of the skin-friction coefficient $C_{f,R}$ for compressible laminar flows at different Mach numbers. The laminar skin-friction coefficient $C_{f,R}$ is not strongly influenced by the change in Mach number, while instead $\mathrm{d}^2F/\mathrm{d}\eta^2|_{\eta=0}$ changes significantly with the Mach number in the adiabatic-wall case. This result is explained by (2.21) because T_w/μ_w appears as a divisor to balance $C_{f,R}$. All the decomposed terms are smaller than $C_{f,R}$ for the isothermal-wall case. For the adiabatic-wall case, however, $sReC_{\theta_v}$ and $sReC_{\bar{\mu}}$ grow rapidly with the Mach number and ultimately overcome $C_{f,R}$ at large Mach number. It is apparent that the decrease of $sReC_\theta$ counteracts the growth of $sReC_{\theta_v}$ and $sReC_{\bar{\mu}}$. The hollow circles are the post-processing data of the incompressible results of EJ, where $sReC_{\bar{\mu}}$ is zero in the incompressible case because the density is constant. The other decomposed terms match our results well.

Figures 1(e) and 1(f) show the downstream development of the decomposed terms. The effects of the Reynolds number and the streamwise coordinate are scaled out, so that the terms are constant along the streamwise direction. The contribution of $sReC_{\bar{\mu}}$ grows gradually with the Mach number and is equal to the sum of $-ReC_\theta$ and $-sReC_{\theta_v}$.

3.2 Skin-friction coefficient of turbulent boundary layers

The decomposition of the skin-friction coefficient of fully-developed turbulent boundary layers is now discussed. The analyzed data are from the direct numerical simulation dataset of Zhang et al. (2018) and Huang et al. (2022). The free-stream velocity is $\mathcal{U}^*_\infty$ =823.6 m/s and the free-stream density is ρ^*_∞ = 0.1 kg/m^3. The free-stream Mach number is $\mathcal{M}_\infty$ = 2.5. The inflow and wall temperatures are T^*_∞ = 270 K and T^*_w = 568 K, respectively. There is no streamwise pressure gradient and the wall temperature is approximately equal to the adiabatic wall recovery temperature. The dependence of the dynamic viscosity on the temperature is modeled by Sutherland's law.

In order to compare the results from a turbulent boundary layer with those from a laminar boundary layer, we need to fix a reference physical quantity for both flows, as in the incompressible case studied by EJ. This quantity can be the streamwise location x, the displacement thickness δ, the momentum thickness θ or the boundary-layer thickness δ_{99}, i.e. the wall-normal distance where the streamwise mean velocity is 99% of the free-stream velocity. The momentum thickness of the laminar boundary layer is

$$\theta = s\int_0^\infty (1-F')\,F'\mathrm{d}\eta = 0.436s. \tag{3.3}$$

We choose the momentum thickness θ as the reference scale for our analysis. It means that we compare the skin friction of a laminar flow with that of a turbulent flow at the same momentum thickness. This choice is preferred to fixing the streamwise location x since a fully developed

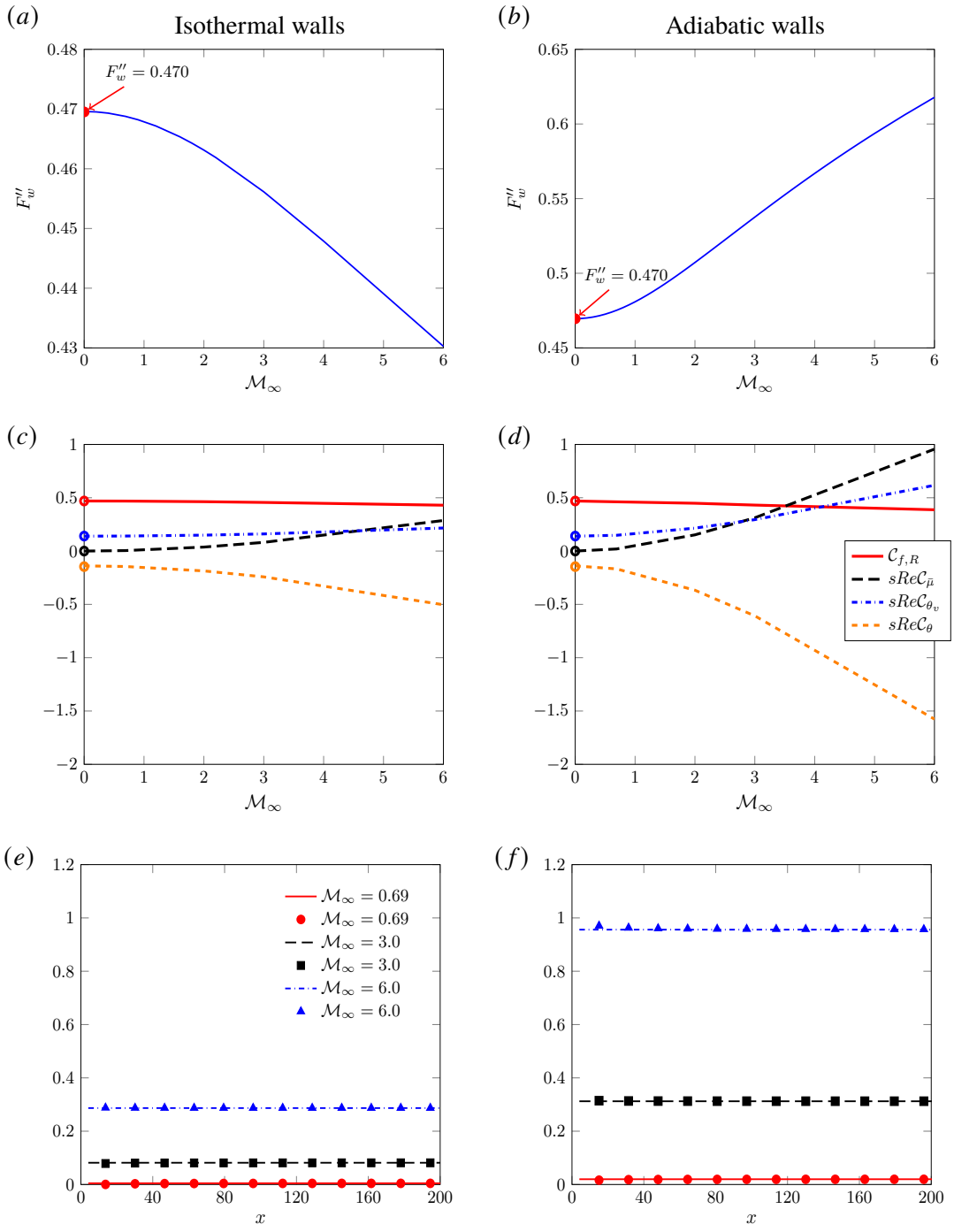

Figure 1: Quantities related to the study of the compressible laminar boundary layer. (a, b) Dependence of $F''_w = \mathrm{d}^2F/\mathrm{d}\eta^2|_{\eta=0}$ on the Mach number. (c, d) Decomposition of skin-friction coefficient $C_{f,R}$ at different Mach numbers. The hollow circles are the scaled incompressible results of EJ. (e, f) Downstream development of the decomposed terms. The lines indicate the contribution of $sReC_{\bar{\mu}}$ and the symbols denote the summation of $-sReC_{\theta}$ and $-sReC_{\theta_v}$. $Pr = 0.707$ and $\gamma = 1.4$.

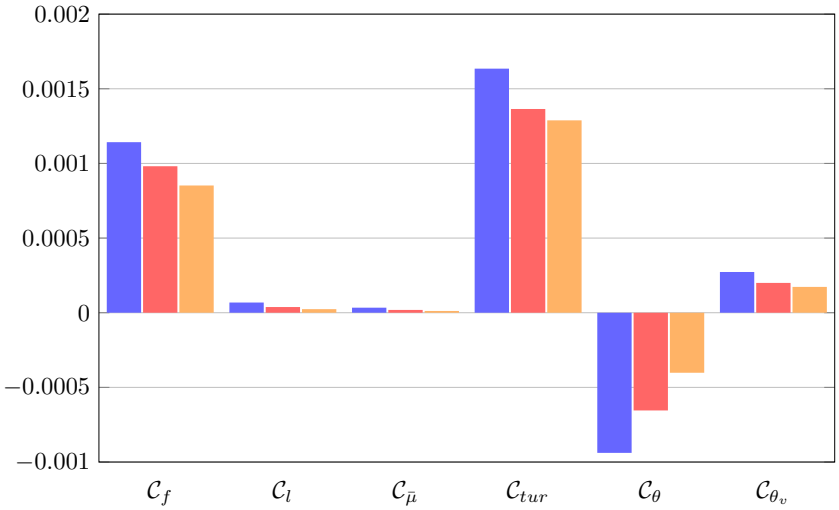

Figure 2: Decomposition of the skin-friction coefficient $C_f/2$ into the terms in (2.15) for a turbulent boundary layer. C_f : Total skin friction; C_l : Laminar contribution; $C_{\bar{\mu}}$: Contribution of viscosity change; C_{tur} : Favre-Reynolds stresses term; C_θ : Boundary-layer growth term; C_{θ_v} : Wall-normal velocity term. The numerical data are from the direct numerical simulations by Zhang et al. (2018) and Huang et al. (2022) at $\mathcal{M}_\infty = 2.5$. The Reynolds numbers are $R_\theta = 2835$ (blue), $R_\theta = 4982$ (red) and R_θ =8093 (yellow).

turbulent boundary layer may be induced artificially at different streamwise locations. Other choices, such as δ and δ_{99}, are possible, but they are not discussed here for brevity.

Figure 2 shows the magnitudes of the terms in identity (2.15) at three different momentum-thickness Reynolds numbers $R_\theta = \rho^*_\infty \mathcal{U}^*_\infty \theta^* / \mu^*_\infty$. The term involving the Favre-Reynolds stresses, C_{tur}, dominates the balance, contributing the most to the wall-shear stress, especially at the lowest Reynolds number which corresponds to the location closest to the leading edge. The term due to the mean-flow streamwise inhomogeneity, C_θ, is the second largest contributor to the balance. Its effect is opposite to that of the Favre-Reynolds stresses: the growth of the boundary layer opposes the enhancement of the wall-shear stress by the Favre-Reynolds stresses by about 40%. The term related to the wall-normal momentum flux, C_{θ_v}, contributes next to the wall-shear stress, i.e. about 25% of the skin-friction coefficient. The impact of the change of viscosity due to the temperature, synthesized by the term $C_{\bar{\mu}}$, and the laminar term C_l are negligible compared to the other terms. The amplitude of all the terms in identity decreases with the Reynolds number.

We note that the identity does not depend on the upper bound of integration because the integration is unbounded along the wall-normal direction. The upper bound instead plays a key role in the various versions of the FIK identity, as verified by Ricco and Skote (2022)

in the incompressible case and discussed in §4 in the compressible case. Moreover, different from the FIK and the RD identities, the laminar contribution to the skin-friction coefficient is distinguished, that is, the skin-friction coefficient reduces to the laminar value when the Favre-Reynolds term vanishes. A further difference is that the RD identity highlights the impact of the terms in the turbulent kinetic equation, while the present identity reveals the influence of the terms in the streamwise momentum equation. Our method could be extended to study the heat-transfer coefficient, similar to the two-fold integration method of WGK.

4 Simplification of alternative Fukagata-Iwamoto-Kasagi identities

Wenzel et al. (2022) and Barone et al. (2022) showed that FIK-like identities quantitatively depend on the upper bound of integration for compressible boundary layers. This dependence was studied in further detail by Ricco and Skote (2022) for incompressible boundary layers. We herein study the identities discovered by Gomez et al. (2009), Wenzel et al. (2022), and Xu et al. (2022) without a streamwise pressure gradient to evince whether the upper integration bound and the number of successive integration impact on the relative contribution of the terms in the identities. We utilize asymptotic methods and the same direct numerical simulation data employed in §3.2.

4.1 Simplification of the three-fold Gomez-Flutet-Sagaut identity

We prove that the identity derived by Gomez et al. (2009) reduces to the compressible von Kármán momentum integral equation when the upper bound of integration is asymptotically large. We choose the local boundary thickness δ^*_{99} as the reference length for this analysis. The Reynolds number is thus $R_\delta = \rho^*_\infty \delta^*_{99} \mathcal{U}^*_\infty / \mu^*_\infty$.

Integrating the Favre-averaged x-momentum equation from 0 to y leads to

$$\bar{\rho}\langle u''v''\rangle - \frac{\bar{\mu}}{R_\delta}\frac{\partial \bar{u}}{\partial y} + \frac{\bar{\mu}}{R_\delta}\frac{\partial \bar{u}}{\partial y}\bigg|_{y=0} + \int_0^y L_x \mathrm{d}y = 0, \tag{4.1}$$

where

$$L_x = \frac{\partial \bar{\rho}\langle u\rangle\langle u\rangle}{\partial x} + \frac{\partial \bar{\rho}\langle u''u''\rangle}{\partial x} + \frac{\partial \bar{\rho}\langle u\rangle\langle v\rangle}{\partial y} - \frac{\partial \bar{\sigma}_{xx}}{\partial x} - \left[\frac{\partial \bar{\sigma}_{yx}}{\partial y} - \frac{1}{R_\delta}\frac{\partial}{\partial y}\left(\bar{\mu}\frac{\partial \bar{u}}{\partial y}\right)\right] + \frac{\partial \bar{p}}{\partial x}. \tag{4.2}$$

For a turbulent boundary layer at high Reynolds number, equation (4.2) reduces to

$$L_x = \frac{\partial \bar{\rho}\langle u\rangle\langle u\rangle}{\partial x} + \frac{\partial \bar{\rho}\langle u\rangle\langle v\rangle}{\partial y} + \frac{\partial \bar{p}}{\partial x}. \tag{4.3}$$

By further integrating (4.1) from 0 to y, we obtain

$$\frac{y\bar{\mu}}{R_\delta}\frac{\partial \bar{u}}{\partial y}\bigg|_{y=0} = -\int_0^y \bar{\rho}\langle u''v''\rangle \mathrm{d}y + \frac{1}{R_\delta}\int_0^y \bar{\mu}\frac{\partial \bar{u}}{\partial y}\mathrm{d}y - \int_0^y \int_0^{\widetilde{y}} L_x \mathrm{d}\hat{y}\mathrm{d}\widetilde{y}. \tag{4.4}$$

Integrating (4.4) from 0 to a wall-normal location h in the free stream, i.e. where $\overline{\rho u} = 1$ and $\overline{\rho v} = 0$, leads to

$$\begin{aligned}\frac{h^2\bar{\mu}}{2R_\delta}\frac{\partial \bar{u}}{\partial y}\bigg|_{y=0} &= -\int_0^h\int_0^y \bar{\rho}\langle u''v''\rangle \mathrm{d}\hat{y}\mathrm{d}y + \frac{1}{R_\delta}\int_0^h\int_0^y \bar{\mu}\frac{\partial \bar{u}}{\partial \hat{y}}\mathrm{d}\hat{y}\mathrm{d}y \\ &\quad -\int_0^h\int_0^y\int_0^{\widetilde{y}} L_x \mathrm{d}\hat{y}\mathrm{d}\widetilde{y}\mathrm{d}y. \end{aligned} \tag{4.5}$$

According to Cauchy's formula for repeated integrations, given in (3.3) of WGK, the skin-friction coefficient can be expressed as

$$\frac{C_f}{2} = \underbrace{-\frac{2}{h^2}\int_0^h (h-y)\bar{\rho}\langle u''v''\rangle \mathrm{d}y}_{\text{Term 1}} + \underbrace{\frac{2}{R_\delta h^2}\int_0^h\int_0^y \bar{\mu}\frac{\partial \bar{u}}{\partial \hat{y}}\mathrm{d}\hat{y}\mathrm{d}y}_{\text{Term 2}} \underbrace{-\frac{1}{h^2}\int_0^h (h-y)^2 L_x \mathrm{d}y}_{\text{Term L3}}, \tag{4.6}$$

where L3 is used to indicate a three-fold integration. If the upper bound h is set equal to 1, that is, $h^* = \delta^*_{99}$, equation (4.6) becomes

$$\begin{aligned} C_f &= \frac{4}{R_\delta}\int_0^1\int_0^y (\widetilde{\mu}+1)\frac{\partial \bar{u}}{\partial \hat{y}}\mathrm{d}\hat{y}\mathrm{d}y - 4\int_0^1 (1-y)\bar{\rho}\langle u''v''\rangle \mathrm{d}y - 2\int_0^1 (y-1)^2 L_x \mathrm{d}y \\ &= \frac{4(1-\delta_d)}{R_\delta} - 4\int_0^1 (1-y)\bar{\rho}\langle u''v''\rangle \mathrm{d}y + \frac{4}{R_\delta}\int_0^1 (1-y)\widetilde{\mu}\frac{\partial \bar{u}}{\partial y}\mathrm{d}y \\ &\quad - 2\int_0^1 (y-1)^2 L_x \mathrm{d}y, \end{aligned} \tag{4.7}$$

where $\widetilde{\mu} = \bar{\mu} - 1$ and $\delta_d = \int_0^1 (1-\bar{u})\mathrm{d}y$. Equation (4.7) agrees with (B1) of GFS if the high-order terms in (B1) are neglected when the boundary-layer theory approximation is adopted (White, 2006). Analogous to the original FIK identity in the incompressible case, the first term on the right-hand side of (4.7) does not correspond to the contribution of a laminar boundary layer. The laminar contribution to the skin-friction coefficient is instead isolated by term C_l in our identity (2.15).

As in the incompressible case of Ricco and Skote (2022), the integration bound h in (4.6) can be taken asymptotically large to remove the dependence of the right-hand side of (4.6) on h. The first and second terms on the right side of (4.6) are null in the limit $h \to \infty$ as the integrals are finite since the corresponding integrands $\bar{\rho}\langle u''v''\rangle$ and $\bar{\mu}\partial\bar{u}/\partial y$ are null in the free stream. It follows that

$$C_f = \lim_{h\to\infty}\left[\underbrace{-\frac{2}{h^2}\int_0^h y^2 L_x \mathrm{d}y}_{\text{Term 3}} + \underbrace{\frac{4}{h}\int_0^h y L_x \mathrm{d}y}_{\text{Term 4}} \underbrace{-2\int_0^h L_x \mathrm{d}y}_{\text{Term 5}}\right], \tag{4.8}$$

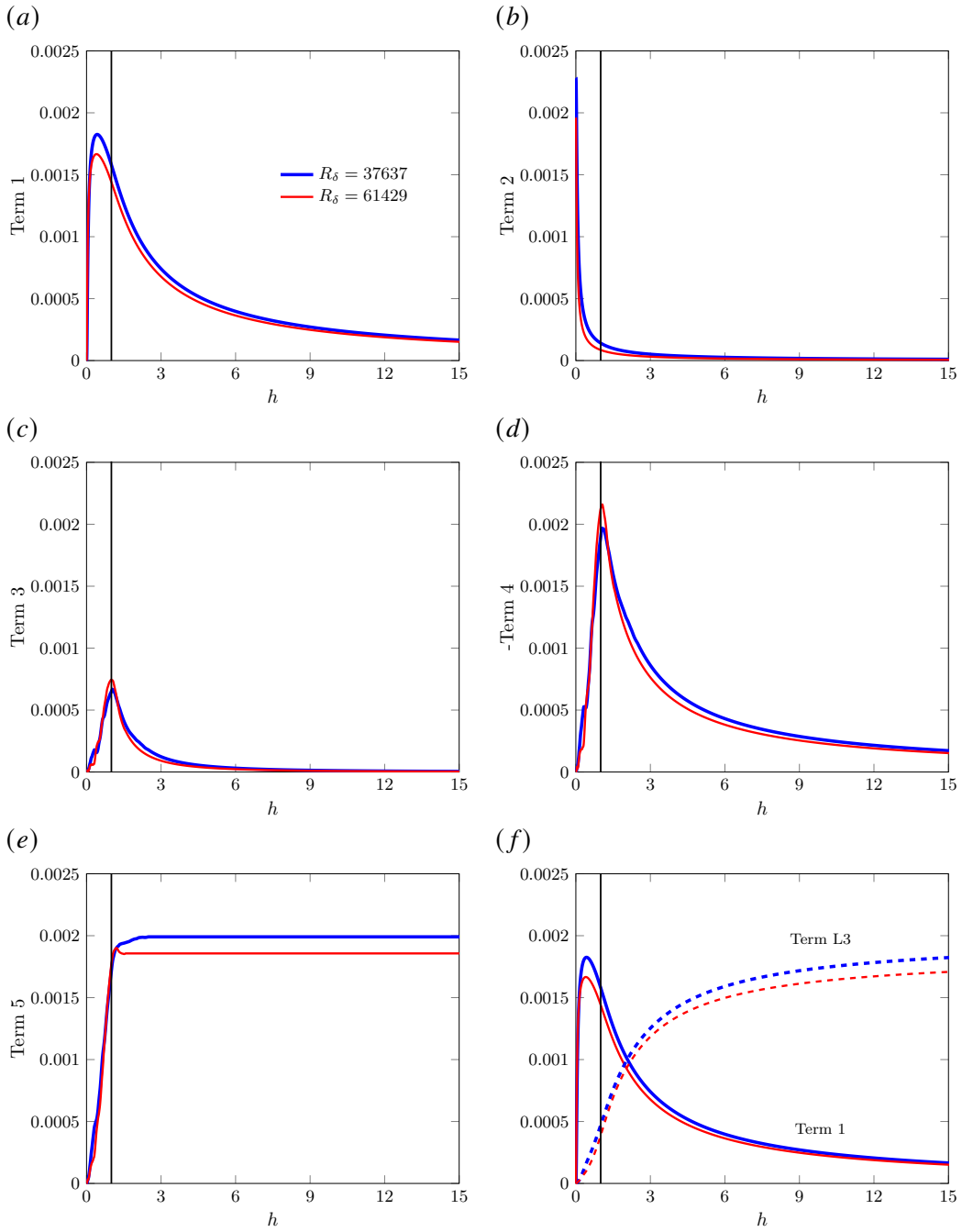

Figure 3: $(a-e)$ Dependence of terms in (4.6) and (4.8) obtained by the three-fold integration on the upper integration bound h for turbulent boundary layers. (f) Comparison of term 1 (solid lines) with term L3 (dashed lines). The numerical data are from the direct numerical simulations by Zhang et al. (2018) and Huang et al. (2022) at $\mathcal{M}_\infty = 2.5$. The vertical line indicates the wall-normal locations where $h = \delta_{99}$.

where the sum of terms 3, 4 and 5 equals term L3 in (4.6). Only term 5 in (4.8) is finite as $h \to \infty$, while terms 3 and 4 are null in this limit, analogous to the incompressible case (Ricco and Skote, 2022). Two cases, at $R_\delta = 37637$ and $R_\delta = 61429$, are studied. These Reynolds numbers correspond to $Re_\tau = 510$ and $Re_\tau = 774$, where Re_τ is the Reynolds number based on the wall-friction velocity, the boundary-layer thickness δ^*_{99}, and the viscosity at the wall. The lower Reynolds number case is from Zhang et al. (2018) and the higher Reynolds number case is from Huang et al. (2022). Figure 3 displays the dependence of terms 1-5 in (4.6) and (4.8) for these two cases on the upper bound h. All the terms vary strongly with h. As h grows asymptotically, terms 1-4 vanish, while term 5 plateaus to a constant.

In the limit $h \to \infty$, equation (4.8) reduces to (A.1),

$$\begin{aligned} \frac{C_f}{2} &= -\int_0^\infty \left(\frac{\partial \bar{\rho}\langle u\rangle\langle u\rangle}{\partial x} + \frac{\partial \bar{\rho}\langle u\rangle\langle v\rangle}{\partial y} + \frac{\partial \bar{p}}{\partial x} \right) \mathrm{d}y \\ &= \int_0^\infty \left[(\rho_e \mathcal{U}_e - \bar{\rho}\langle u\rangle) \frac{\mathrm{d}\mathcal{U}_e}{\mathrm{d}x} + \frac{\partial (\mathcal{U}_e - \langle u\rangle)\bar{\rho}\langle u\rangle}{\partial x} \right] \mathrm{d}y. \end{aligned} \tag{4.9}$$

To obtain (4.9), we have utilized (2.11) and neglected the pressure-fluctuation term $-\partial\overline{p'}/\partial x = \partial\left(\overline{\rho}\langle v''^2\rangle\right)/\partial x$ emerging from the y-momentum equation because it is small in a high-Reynolds-number turbulent boundary layer (Bradshaw, 1964). We have also used $\int_0^\infty \partial\left(\bar{\rho}\langle u\rangle\right)/\partial x \, \mathrm{d}y = 0$, which follows from the continuity equation. Equation (4.9) therefore simplifies to (A.2), which indicates that, in the case of a compressible boundary layer, the GFS identity reduces to the compressible von Kármán momentum integral equation.

In the original FIK identity for incompressible boundary layers, δ^*_{99} was the upper bound of choice. However, in the compressible FIK identities, such as those proposed by WGK and XWC, the upper bound has been chosen to be larger than δ^*_{99} because of the need to select a domain that covers the thermal boundary layer as well, especially in the case of hypersonic boundary layers. This issue does not concern the analysis of incompressible boundary layers because no thermal effects incur in that case. In view of this idea, attention should be paid to figure 3(f), where the turbulent term 1 is compared with the spatial-growth term L3, defined in (4.6). Figure 3(f) and the analogous figure 4(f) were not shown in the incompressible analysis by Ricco and Skote (2022). The turbulent term 1 shows a rapid decrease near δ_{99}, while the spatial-growth term L3 grows significantly there. These terms match at $h \approx 2\delta_{99}$ and the spatial-growth term L3 dominates for $h{>}2\delta_{99}$. The balance is therefore dominated by the turbulent term if h chosen to be comparable with δ_{99} and by the spatial-growth term if h is taken to be larger than $2\delta_{99}$. This crossover occurring as the upper bound increases therefore leads to totally different qualitative and quantitative conclusions about the impact of the different terms of the streamwise momentum equation on the wall friction.

As shown in figures 3(a) and 3(b), since the contributions of the Favre-Reynolds stresses and $\bar{\mu}\partial\bar{u}/\partial y$ to the skin-friction coefficient vanish in the limit $h{\to}\infty$, it is thus not possible to quantify the impact of these different terms on the wall friction. This problem arises because the geometry

of the system does not possess a precise scale along the wall-normal direction, differently from channel and pipe flows, for which the channel height and the pipe radius are instead used as upper integration bounds. It follows that the skin-friction coefficient depends spuriously on h because h is a mathematical quantity used to derive the identity. We also conclude that the GFS identity does not allow for the quantification of the contribution of the Favre-Reynolds stresses to the skin-friction coefficient.

4.2 Simplification of the two-fold Wenzel-Gibis-Kloker identity

The FIK and GFS identities are based on a three-fold integration of the streamwise momentum equation. For compressible turbulent boundary layers, WGK and XWC instead decomposed the skin-friction coefficient by a two-fold integration. The two-fold integration of the streamwise momentum equation leads to the identity

$$C_f = \underbrace{-\frac{2}{h}\int_0^h \bar{\rho}\langle u''v''\rangle \mathrm{d}y}_{\text{Term I}} + \underbrace{\frac{2}{hR_\delta}\int_0^h \bar{\mu}\frac{\partial \bar{u}}{\partial y}\mathrm{d}y}_{\text{Term II}} + \underbrace{2\int_0^h (y-h)L_x \mathrm{d}y}_{\text{Term L2}}, \tag{4.10}$$

where the last term can be written as

$$\mathrm{L2} = 2\int_0^h (y-h)L_x \mathrm{d}y = \underbrace{\frac{2}{h}\int_0^h yL_x \mathrm{d}y}_{\text{Term III}} \underbrace{-2\int_0^h L_x \mathrm{d}y}_{\text{Term IV}}. \tag{4.11}$$

The terms on the right-hand side of (4.10) depend on the integration bound h, as in the GFS identity. In the limit $h \to \infty$, terms I and II in (4.10) are null because the integrals are finite as the Favre-Reynolds stresses and $\bar{\mu}\partial\bar{u}/\partial y$ are null in the free stream. The integrand yL_x in term III of (4.11) is zero outside of the boundary layer and hence its integral is finite as well. It follows that term III approaches zero when $h \to \infty$. Term IV instead contributes to the skin-friction coefficient by itself in the limit $h \to \infty$. Term IV coincides with term 5 in (4.8), which arises from the three-fold integration, and, similar to the three-fold GFS identity, the two-fold identity obtained by WGK also reduces to the compressible von Kármán momentum integral equation when $h \to \infty$.

Figure 4 unveils the contributions of terms I-IV in (4.10) and (4.11) on the upper integration bound h. Terms I-III exhibit an intense dependence on h and tend to 0 as $h \to \infty$. The Favre-Reynolds stresses (term I) are excluded from the contribution of the skin-friction coefficient if an asymptotically large upper bound is chosen. Term IV instead grows to a constant as $h \to \infty$. The decay of term I and the rapid growth of term IV are evident near $h = 1$, i.e. at the edge of the boundary layer, which indicates that the two-fold identity is sensitive to the upper bound at around $h = 1$. As for the three-fold identity, the terms of the identity depend spuriously on the upper bound. The turbulent term I is compared to the spatial-development term L2 in figure 4(e). The turbulent term I is smaller than term L2 for $h < 0.8\delta_{99}$, but the spatial-development term

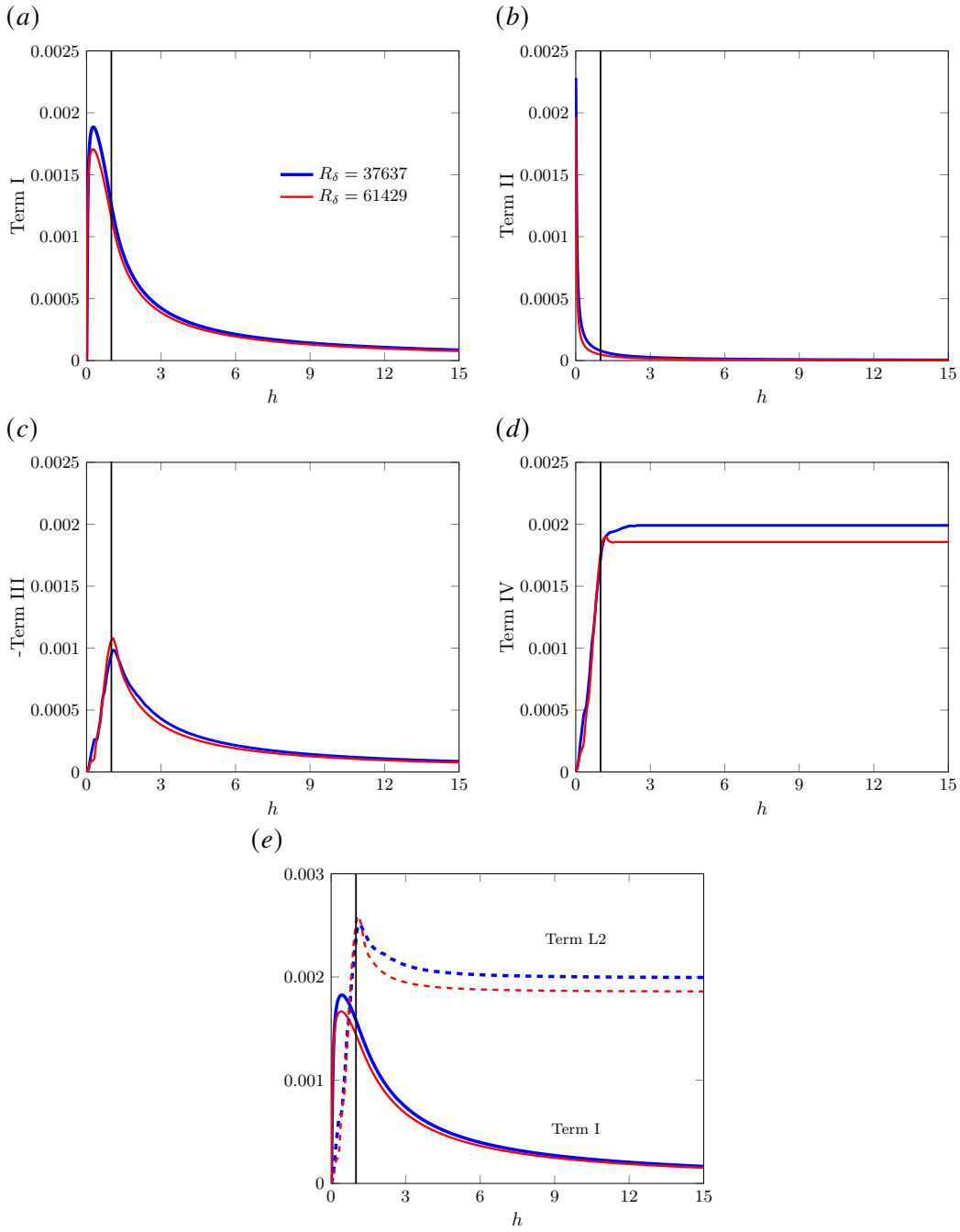

Figure 4: $(a-d)$ Dependence of terms I-IV (4.10-4.11) obtained by the two-fold integration on the upper integration bound h for turbulent boundary layers at two Reynolds numbers. (e) Comparison of term I (solid lines) with term L2 (dashed lines). The vertical line indicates the wall-normal location where $h = \delta_{99}$. The parameters are the same as the direct numerical simulation data of Zhang et al. (2018) and Huang et al. (2022) for $\mathcal{M}_\infty = 2.5$.

L2 dominates for $h > 0.8\delta_{99}$. It should be noted that the value of h where the turbulent term I equals term L2 changes for different cases. It can be larger than δ_{99}, as in the case of the three-fold-integration GFS identity shown in figure 3(f). The conclusion is that a slight modification of the upper bound can drastically change the dominant term in the two-fold integration identity. This significant change does not happen for the identity (2.15) as it does not depend on the upper bound.

Thanks to these results, we are now in the position to analyze the results of WGK and XWC. To include all the dynamical effects of a compressible boundary layer, WGK and XWC set the upper integration bound to $1.3\delta^*_{99}$ and $1.5\delta^*_{99}$, respectively. The boundary-layer dynamics, and therefore its kinematic thickness and its thermal thickness, is related to the Mach number and the wall temperature, and hence, to apply this theoretical framework, the upper integration limit should change in each case in order to include all the dynamical and thermal features of the boundary layer. WGK showed that the decomposed terms are sensitive to the upper integration bound, as revealed by their figure 12.

Terms I-IV in (4.10) and (4.11) are related to the terms in the identities by WGK and XWC. Term I in (4.10) is the turbulent-convection term c_f^T in (3.7) of WGK. Term II is the boundary-layer term c_f^L of WGK. The last term in (4.10) can be interpreted as the sum of the mean-convection term c_f^M and the spatial-development term c_f^D ($\partial\bar{p}/\partial x = 0$ for their case). Equation (3.7) in WGK is the same as our (4.6), if one combines c_f^M and c_f^D to our third term in the right of our (4.6) and takes $\partial\bar{p}/\partial x = 0$. The dependence of the decomposed terms on the upper bound can be misleading. WGK showed that the dominant term is the turbulent-convection term c_f^T (our term I) when the upper bound is $h^* = 1.3\delta^*_{99}$, whereas the spatial-development c_f^D (part of our term L2) becomes dominant when the upper bound is chosen to be $h^* = 2\delta^*_{99}$ (refer to their figure 12).

The terms in equation (3.4) of XWC include high-order terms. The term C_f^B of XWC is our term II as we neglect high-order terms. Their term C_f^T is our term I. The combination of $C_f^{D,1}$, $C_f^{D,2}$ and $C_f^{D,3}$ is L2, the last term of our (4.10). The numerical results of XWC showed that the spatial-development term is dominant. XWC reported the spatial-development term to be dominant and concluded that the overshoot of the skin-friction coefficient is mainly caused by the streamwise dependence of the mean-flow profiles and not by the Reynolds stresses. This conclusion can be questioned because one can specify a smaller upper bound of integration to mitigate the contribution of the spatial-development term. The contribution of the terms to the dynamical balance and to the wall-shear stress should not depend on the upper integration bound because h is arbitrary.

We also note that the identity (2.15) simplifies to the two-fold identity (4.10) by neglecting the streamwise pressure gradient and setting $\mathscr{L}$ and the upper integration bounds of both equations equal to 1.

4.3 Simplification of the multifold Wenzel-Gibis-Kloker identity

The identity emerging from a number of successive integrations n between 0 and y performed before the final integration between 0 and h was studied by Ricco and Skote (2022) for an incompressible channel flow and by WGK for a compressible turbulent boundary layer. Ricco and Skote (2022) studied the asymptotic behavior of the repeated-integration identity as $n \to \infty$ and proved that the integral involving the Reynolds stresses impacts less and less on the skin-friction coefficient as n increases because that term behaves $\sim 48A_{uv3}/n^3$, where A_{uv3} is a constant. A key conclusion was that the channel-flow identity only possesses a defined physical meaning in the original FIK case. We now utilize the asymptotic method of Ricco and Skote (2022) to study the multifold WGK identity as $h \to \infty$ and $n \to \infty$ and investigate the behavior of the different terms in these limits.

As shown by WGK, a number n of successive integrations between 0 and y can be performed on (4.1) before the final integration between 0 and h, to obtain

$$\begin{aligned} C_f = \quad & \underbrace{-\frac{2n}{h^n}\int_0^h (h-y)^{n-1}\bar{\rho}\langle u''v''\rangle \mathrm{d}y}_{\text{Term A}} + \underbrace{\frac{2n}{h^n R_\delta}\int_0^h (h-y)^{n-1}\bar{\mu}\frac{\partial \bar{u}}{\partial y}\mathrm{d}y}_{\text{Term B}} \\ & \underbrace{-\frac{2}{h^n}\int_0^h (h-y)^n L_x \mathrm{d}y}_{\text{Term C}}. \end{aligned} \tag{4.12}$$

In the limit $h \to \infty$, the first term and the second term on the right-hand side of (4.12) become negligible because the integral always grows more slowly than the denominator h^n. The third term is dominant and can be expanded by using the binomial theorem,

$$-\frac{2}{h^n}\int_0^h (h-y)^n L_x \mathrm{d}y = -2\sum_{k=0}^{n}\binom{n}{k}\frac{(-1)^k}{h^k}\int_0^h y^k L_x \mathrm{d}y. \tag{4.13}$$

When $h \to \infty$, the terms on the right-hand of (4.13) for $k \neq 0$ become negligible because the integrals are finite. The term for $k = 0$ is finite since it is independent of h. We adopt the boundary-layer assumption and hence the non-homogenous term (4.2) reduces to (4.3). In the limit $h \to \infty$, the skin-friction coefficient is

$$\frac{C_f}{2} = -\int_0^\infty L_x \mathrm{d}y = -\int_0^\infty \frac{\partial \bar{\rho}\langle u\rangle\langle u\rangle}{\partial x}\mathrm{d}y = \frac{\mathrm{d}}{\mathrm{d}x}\int_0^\infty (1-\bar{\rho}\langle u\rangle\langle u\rangle)\,\mathrm{d}y = \frac{\mathrm{d}\theta}{\mathrm{d}x}, \tag{4.14}$$

which is equal to (A.2) if one takes $\mathcal{U}_e = 1$. It follows that the WGK multifold identity (4.12) reduces to the compressible von Kármán momentum integral equation.

We now study the case for $h = 1$, which corresponds to $h^* = \delta^*_{99}$, and the limit $n \to \infty$. By using the change of variable $s = -\ln(1-y)$, the skin-friction coefficient becomes

$$C_f = -2n\int_0^\infty \bar{\rho}\langle u''v''\rangle e^{-ns}\mathrm{d}s + \frac{2n}{R_\delta}\int_0^\infty \bar{\mu}\frac{\partial \bar{u}}{\partial y}e^{-ns}\mathrm{d}s - 2\int_0^\infty L_x e^{-s}e^{-ns}\mathrm{d}s. \tag{4.15}$$

We expand the Favre-Reynolds stresses, the mean shear-stress term and the convection term L_x in (4.15) for $s \to 0^+$,

$$\begin{aligned}
\bar{\rho}\langle u''v''\rangle &\sim A_3 y^3 + A_4 y^4 + O(y^5) = A_3(1-e^{-s})^3 + A_4(1-e^{-s})^4 + \dots \\
&= s^3\left[A_3 + (A_4 - 3A_3)\, s\right] + O(s^5), \qquad (4.16)\\
\bar{\mu}\frac{\partial \bar{u}}{\partial y} &\sim B_0 + B_1 y + B_2 y^2 + O(y^3) = B_0 + B_1(1-e^{-s}) + B_2(1-e^{-s})^2 + \dots \\
&= B_0 + B_1 s + \left(B_2 - \frac{B_1}{2}\right) s^2 + O(s^3), \qquad (4.17)\\
L_x e^{-s} &\sim \left(\bar{\rho}\langle u\rangle \frac{\partial \langle u\rangle}{\partial x} + \bar{\rho}\langle v\rangle \frac{\partial \langle u\rangle}{\partial y}\right) e^{-s} = \left[C_2 y^2 + C_3 y^3 + O(y^4)\right] e^{-s} \\
&= \left[C_2(1-e^{-s})^2 + C_3(1-e^{-s})^3 + \dots\right] e^{-s} \\
&= C_2 s^2 + (C_3 - 2C_2)\, s^3 + O(s^4), \qquad (4.18)
\end{aligned}$$

where

$$\langle u\rangle = a_1 y + a_2 y^2 + O(y^3), \quad \langle v\rangle = b_2 y^2 + b_3 y^3 + O(y^4), \qquad (4.19)$$

$$\langle \rho\rangle = c_0 + c_1 y + O(y^2), \quad \bar{\rho}\langle u\rangle \frac{\partial \langle u\rangle}{\partial x} = O(y^2), \quad \bar{\rho}\langle v\rangle \frac{\partial \langle u\rangle}{\partial y} = O(y^2). \qquad (4.20)$$

The coefficients $A_n(R_\delta)$, $B_n(R_\delta)$ and $C_n(R_\delta)$ can be determined numerically. For $R_\delta = 37637$,

$$\begin{aligned}
&A_3 = -299.36,\ A_4 = 3563.35,\ B_0 = 42.99,\ B_1 = -44.80,\\
&C_0 = -1.01,\ C_1 = -1.56,
\end{aligned}$$

while for $R_\delta = 61429$

$$\begin{aligned}
&A_3 = -1251.03,\ A_4 = 39668.72,\ B_0 = 60.27,\ B_1 = -66.51,\\
&C_0 = -2.20,\ C_1 = 154.50.
\end{aligned}$$

Using Watson's lemma (Bender and Orszag, 1999) leads to

$$\begin{aligned}
C_f \;\sim\; & -2n\left[\frac{\Gamma(4)A_3}{n^4} + \left(A_4 - \frac{3A_3}{2}\right)\frac{\Gamma(5)}{n^5} + \dots\right] - 2\left[\frac{\Gamma(3)C_2}{n^3} + (C_4 - 2C_3)\,\frac{\Gamma(4)}{n^4} + \dots\right] \\
+ \;& \frac{2n}{R_\delta}\left[\frac{\Gamma(1)B_0}{n} + \frac{\Gamma(2)B_1}{n^2} + \left(B_2 - \frac{B_1}{2}\right)\frac{\Gamma(3)}{n^3} + \dots\right] \sim \frac{2\bar{\mu}}{R_\delta}\left.\frac{\partial \bar{u}}{\partial y}\right|_{y=0}, \qquad (4.21)
\end{aligned}$$

where Γ is the Gamma function. As n grows, the skin-friction coefficient approaches B_0/R_δ, ruling out the contribution of the Favre-Reynolds stresses at leading order. It also follows that the identity collapses to the definition of the skin-friction coefficient itself, therefore revealing no information about the dynamics of the flow and proving that the dependence on n is spurious.

Figure 5 shows the dependence of the terms composing the WGK multifold identity on the integration number n. The Favre-Reynolds stress term A first increases, reaches a peak value

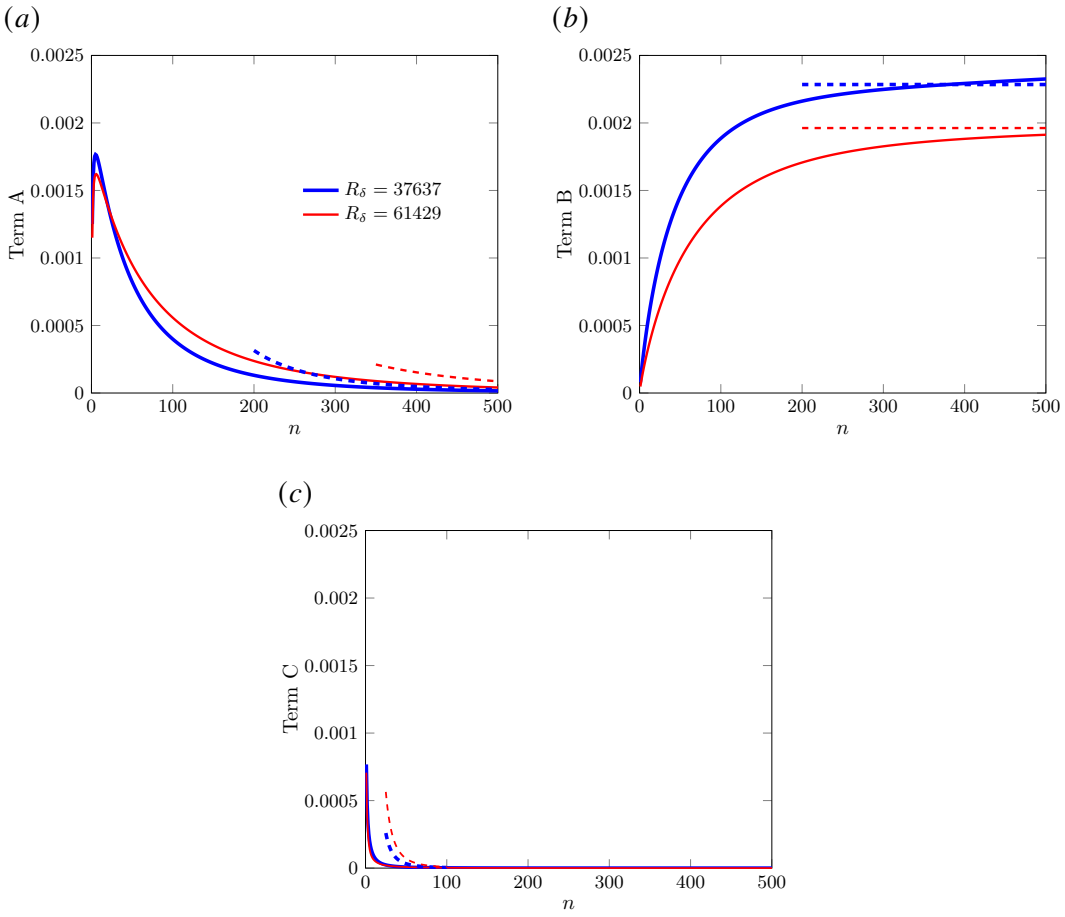

Figure 5: Dependence of terms A (graph a), B (graph b) and C (graph c) in (4.12) on the number of iterations n for turbulent boundary layers at two Reynolds numbers. The solid and dashed lines correspond to the numerical and asymptotic solutions, respectively. The parameters are the same as the direct numerical simulation data of Zhang et al. (2018) and Huang et al. (2022). The Mach number is $\mathcal{M}_\infty = 2.5$.

at $n = 15$ and then decreases slowly. The non-homogeneous term C rapidly decays to zero as n increases. The mean-flow term B is dominant for large n, rather than the non-homogeneous term for the two-fold or the three-fold decomposition when the large-h limit is taken. The present results explain the cases studied in figure 11 of WGK. The maximum value of n in WGK is 10, for which the contribution of the Favre-Reynolds stresses is significant, as displayed in figure 5. If WGK had chosen a larger value of n, the Favre-Reynolds stress term would have been less impactful on the skin-friction coefficient. It is clear that the Favre-Reynolds stress term is sensitive to the integration number n, a further indication that the influence of n on the contribution of the different terms on the wall friction is spurious.

5 Conclusions

In this paper, we have derived an integral formula for the skin-friction coefficient of compressible boundary layers that isolates the contribution of the laminar skin-friction coefficient, the Favre-Reynolds stresses, the mean-flow streamwise inhomogeneity and the change of viscosity due to the temperature gradients. This identity is the compressible-flow version of that obtained by Elnahhas and Johnson (2022) for incompressible boundary layers. It allows for the quantification of the contribution of different terms in the streamwise momentum equation to the wall-shear stress. The identity removes the dependence on the upper bound of integration and is therefore valid for compressible boundary layers with an unbounded domain in the wall-normal direction. Just like the incompressible counterpart proposed by Elnahhas and Johnson (2022) and the identity proposed by Renard and Deck (2016), the derivation adopts an unbounded integration along the wall-normal direction.

The three-fold repeated integration identity of Gomez et al. (2009), which is the compressible version of the incompressible identity found by Fukagata et al. (2002), and the two-fold repeated integration identities of Wenzel et al. (2022) and Xu et al. (2022) all simplify to the compressible von Kármán momentum integral equation when the upper limit of integration is asymptotically large. We have also proved that the upper integration bound used to derive the identities has a significant impact on the contribution of the terms of the streamwise momentum equation on the wall friction. Therefore, this problem prevents the use of these identities for the quantification of the effect of the Favre-Reynolds stresses on the wall friction.

The multifold integral method of Wenzel et al. (2022) was studied, too. Their identity also reduces to the von Kármán momentum integral equation for an asymptotically large integration bound. As the number of integrations becomes asymptotically large, we have proved by asymptotic methods that the identity degenerates to the definition of the skin-friction coefficient, revealing no information about the physics of the boundary layer.

In the analysis of a Mach 2.5 turbulent boundary layer with an adiabatic wall, our new integral identity shows that the Favre-Reynolds stresses dominate the boundary-layer dynamics, contributing the most to the skin-friction coefficient. The mean-flow streamwise inhomogeneity

has an opposite effect on the wall friction to that of the Favre-Reynolds stresses, while the wall-normal momentum flux has a smaller impact. The term due to the temperature-dependent viscosity and the laminar term are negligible. All the terms in the identity decrease with the Reynolds number except for the term related to the mean-flow streamwise inhomogeneity.

The identity will serve the useful purpose of computing the wall-shear stress of a compressible turbulent boundary layer by post-processing experimental data measured along the wall-normal direction. This application of the identity is particularly noteworthy in the compressible regime, where obtaining the wall-shear stress by directly measuring the velocity gradient at the wall is an immense challenge (Goyne et al., 2003). The identity could also be helpful to evince how flow-control methods, designed for example to attenuate the wall friction, modify the momentum and energy transfer in a turbulent boundary layer. Compressible transitional boundary layers can also be investigated by using the method developed herein (Zhou et al., 2022; Tong et al., 2022; Chen et al., 2022).

Acknowledgments

DX thanks Dr Lei Zhao from Tianjin University for useful discussions. DX and PR acknowledge the support of EPSRC (Grant No. EP/T01167X/1) and would like to thank Mr Ludovico Fossá for the useful comments. PR has also been supported by the US Air Force through the AFOSR grant FA8655-21-1-7008 (International Program Office Dr Douglas Smith).

A The compressible von Kármán momentum integral equation

The compressible von Kármán momentum integral equation is derived as follows. Integrating (2.12) from the wall to infinity leads to

$$\begin{aligned}\left.\frac{\bar{\mu}}{Re}\frac{\partial\bar{u}}{\partial y}\right|_{y=0} =& \int_0^\infty \left[\left(\rho_e\mathcal{U}_e-\bar{\rho}\langle u\rangle\right)\frac{\mathrm{d}\mathcal{U}_e}{\mathrm{d}x}+\frac{\partial\left(\mathcal{U}_e-\langle u\rangle\right)}{\partial x}\bar{\rho}\langle u\rangle\right]\mathrm{d}y\\ =&\rho_e\mathcal{U}_e\frac{\mathrm{d}\mathcal{U}_e}{\mathrm{d}x}\int_0^\infty\left(1-\frac{\bar{\rho}\langle u\rangle}{\rho_e\mathcal{U}_e}\right)\mathrm{d}y+\frac{\mathrm{d}\left(\rho_e\mathcal{U}_e^2\right)}{\mathrm{d}x}\int_0^\infty\left(1-\frac{\langle u\rangle}{\mathcal{U}_e}\right)\frac{\bar{\rho}\langle u\rangle}{\rho_e\mathcal{U}_e}\mathrm{d}y\\ &+\rho_e\mathcal{U}_e^2\frac{\mathrm{d}\theta}{\mathrm{d}x}.\end{aligned} \tag{A.1}$$

By considering a free-stream potential flow with constant density $\rho_e = 1$ and streamwise-varying $\mathcal{U}_e$, equation (A.1) becomes the compressible von Kármán momentum integral equation

$$\frac{C_f}{2}=\frac{\mathrm{d}\theta}{\mathrm{d}x}+\frac{\delta+2\theta}{\mathcal{U}_e}\frac{\mathrm{d}\mathcal{U}_e}{\mathrm{d}x}, \tag{A.2}$$

where

$$\delta(x)\equiv\int_0^\infty\left(1-\frac{\bar{\rho}\langle u\rangle}{\rho_e\mathcal{U}_e}\right)\mathrm{d}y \quad\text{and}\quad \theta(x)\equiv\int_0^\infty\left(1-\frac{\langle u\rangle}{\mathcal{U}_e}\right)\frac{\bar{\rho}\langle u\rangle}{\rho_e\mathcal{U}_e}\mathrm{d}y \tag{A.3}$$

are the compressible displacement thickness and momentum thickness, respectively. Equation (A.2) is the scaled form of (7-61) of White (2006) when their parameter Ma_e is null.

B The compressible laminar boundary-layer solution

The compressible Blasius boundary layer without a streamwise pressure gradient possesses a similarity solution (Stewartson, 1964),

$$u = U = F'(\eta), \quad v = V = \frac{T(\eta_c F' - F)}{\sqrt{2xRe}}, \quad T = T(\eta). \tag{B.1}$$

where $\eta_c = T^{-1}\int_0^\eta T(\check{\eta})\mathrm{d}\check{\eta}$, the similarity variable η is

$$\eta = \frac{1}{s}\int_0^y \rho(x,\check{y})\mathrm{d}\check{y},$$

and s is defined in (2.21). The prime denotes differentiation with respect to η. The compressible Blasius functions $F(\eta)$ and $T(\eta)$ are determined by the boundary-value problem

$$\left.\begin{array}{c} (\mu F''/T)' + FF'' = 0 \\ (\mu T'/T)' + PrFT' + \mu(\gamma-1)Pr\mathcal{M}_\infty^2(F'')^2/T = 0, \\ F = F' = 0, \quad \text{at} \quad \eta = 0, \\ F' = 1, \quad T' = 0, \quad \text{as} \quad \eta \to \infty, \end{array}\right\} \tag{B.2}$$

where the Prandtl number $Pr = 0.707$ and the dynamic viscosity $\mu(T) = T^\omega$ with $\omega = 0.76$ (Stewartson, 1964). The power law is adopted for the dynamic viscosity in the analysis of the laminar boundary layer, although the decomposition of the skin-friction coefficient is valid for any viscosity law. The boundary conditions for the wall temperature are $T = T_w$ and $T'(0) = 0$ for isothermal and adiabatic walls, respectively.

For a zero-pressure-gradient boundary layer, the displacement thickness and the momentum thickness (A.3) reduce to

$$\delta(x) \equiv s\int_0^\infty \left(1 - \frac{F'}{T}\right) T\mathrm{d}\eta \quad \text{and} \quad \theta(x) \equiv s\int_0^\infty (1-F')\,F'\mathrm{d}\eta. \tag{B.3}$$

The skin-friction coefficient is proportional to $1/\sqrt{x}$, as shown by (6.71) of Anderson (2000). The decomposition of the skin-friction coefficient for a laminar boundary layer simplifies to

$$\frac{C_f}{2} = \underbrace{\frac{1}{Re_{\mathscr{C}}}}_{C_l} + \underbrace{\frac{-1}{Re_{\mathscr{C}}}\int_0^\infty \frac{\mathrm{d}\mu}{\mathrm{d}T}T'F'\mathrm{d}\eta}_{C_{\bar{\mu}}} + \underbrace{\frac{\mathrm{d}\theta_{\mathscr{C}}}{\mathrm{d}x} - \frac{\theta-\theta_{\mathscr{C}}}{\mathscr{C}}\frac{\mathrm{d}\mathscr{C}}{\mathrm{d}x}}_{C_\theta} + \underbrace{\frac{\theta_v}{\mathscr{C}}}_{C_{\theta_v}}, \tag{B.4}$$

where $C_{\bar{\mu}} + C_\theta + C_{\theta_v} = 0$. The momentum thicknesses reduce to

$$\theta_{\mathscr{C}}(x) = s\int_0^\infty \left(1 - \frac{y}{\mathscr{C}}\right)(1-F')\,F'\mathrm{d}\eta \quad \text{and} \quad \theta_v = \frac{1}{Re}\int_0^\infty (1-F')\,(\eta_c F' - F)T\mathrm{d}\eta,$$

where $y/\mathscr{C}$ is a function of η and is expressed as

$$\frac{y}{\mathscr{C}} = \frac{\mu_w}{T_w}\frac{\partial^2 F}{\partial \eta^2}\Big|_{\eta=0}\int_0^{\eta} T(\check{\eta})\mathrm{d}\check{\eta}.$$

For a laminar boundary layer, the terms are

$$C_l \propto \frac{1}{\mathscr{C}} \propto \frac{1}{\sqrt{x}}, \quad C_{\bar{\mu}} \propto \frac{1}{\sqrt{x}}, \quad C_\theta \propto \frac{1}{\sqrt{x}}, \quad C_{\theta_v} \propto \frac{1}{\sqrt{x}}. \tag{B.5}$$

References

Adumitroaie, V., Ristorcelli, J. R., and Taulbee, D. B. (1999). Progress in Favré–Reynolds stress closures for compressible flows. *Phys. Fluids*, 11(9):2696–2719.

Anderson, J. D. (2000). *Hypersonic and high temperature gas dynamics*. AIAA - Education Series - 2nd edition.

Barone, M., Nicholson, G. L., and Duan, L. (2022). Internal energy balance and aerodynamic heating predictions for hypersonic turbulent boundary layers. *Phys. Rev. F*, 7(8):084604.

Bender, C. M. and Orszag, S. A. (1999). *Advanced mathematical methods for scientists and engineers I: Asymptotic methods and perturbation theory*. Springer Science & Business Media, New York.

Bradshaw, P. (1964). *Experimental Fluid Mechanics*. Pergamon Press.

Chen, X., Chen, J., and Yuan, X. (2022). Hypersonic boundary layer transition on a concave wall induced by low-frequency blowing and suction. *Phys. Fluids*, 34(11):114105.

Elnahhas, A. and Johnson, P. L. (2022). On the enhancement of boundary layer skin friction by turbulence: an angular momentum approach. *J. Fluid Mech.*, 940.

Fan, Y., Li, W., and Pirozzoli, S. (2019). Decomposition of the mean friction drag in zero-pressure-gradient turbulent boundary layers. *Phys. Fluids*, 31(8):086105.

Favre, A. J. (1965). The equations of compressible turbulent gases. Technical Report AD0622097., DTIC Document.

Favre, A. J. (1992). Formulation of the statistical equations of turbulent flows with variable density. In *Studies in turbulence*, pages 324–341. Springer.

Fukagata, K., Iwamoto, K., and Kasagi, N. (2002). Contribution of Reynolds stress distribution to the skin friction in wall-bounded flows. *Phys. Fluids*, 14(11):L73–L76.

Gomez, T., Flutet, V., and Sagaut, P. (2009). Contribution of Reynolds stress distribution to the skin friction in compressible turbulent channel flows. *Phys. Rev. E*, 79(3):035301.

Goyne, C., Stalker, R., and Paull, A. (2003). Skin-friction measurements in high-enthalpy hypersonic boundary layers. *J. Fluid Mech.*, 485:1–32.

Huang, G., Si, W., and Lee, C. (2021). Inner structures of Görtler streaks. *Phys. Fluids*, 33(3):034116.

Huang, J., Duan, L., and Choudhari, M. M. (2022). Direct numerical simulation of hypersonic turbulent boundary layers: effect of spatial evolution and Reynolds number. *J. Fluid Mech.*, 937.

Marensi, E., Ricco, P., and Wu, X. (2017). Nonlinear unsteady streaks engendered by the interaction of free-stream vorticity with a compressible boundary layer. *J. Fluid Mech.*, 817:80–121.

Renard, N. and Deck, S. (2016). A theoretical decomposition of mean skin friction generation into physical phenomena across the boundary layer. *J. Fluid Mech.*, 790:339–367.

Ricco, P. and Skote, M. (2022). Integral relations for the skin-friction coefficient of canonical flows. *J. Fluid Mech.*, 943(A50).

Stewartson, K. (1964). *The theory of laminar boundary layers in compressible fluids*. Clarendon Press Oxford.

Tong, F., Dong, S., Lai, J., Yuan, X., and Li, X. (2022). Wall shear stress and wall heat flux in a supersonic turbulent boundary layer. *Phys. Fluids*, 34(1):015127.

von Kármán, T. (1946). Über laminare und turbulente Reibung. *Angew. Math. Mech*, 1:233–252.

Wenzel, C., Gibis, T., and Kloker, M. (2022). About the influences of compressibility, heat transfer and pressure gradients in compressible turbulent boundary layers. *J. Fluid Mech.*, 930:A1.

White, F. M. (2006). *Viscous fluid flow*. McGraw-Hill, New York.

Xu, D., Wang, J., and Chen, S. (2022). Skin-friction and heat-transfer decompositions in hypersonic transitional and turbulent boundary layers. *J. Fluid Mech.*, 941.

Zhang, C., Duan, L., and Choudhari, M. M. (2018). Direct numerical simulation database for supersonic and hypersonic turbulent boundary layers. *AIAA J.*, 56(11):4297–4311.

Zhou, T., Liu, Z., Lu, Y., Wang, Y., and Yan, C. (2022). Direct numerical simulation of complete transition to turbulence via first-and second-mode oblique breakdown at a high-speed boundary layer. *Phys. Fluids*, 34(7):074101.